


Article

Greater Greening Trend in the Loess Plateau of China Inferred from Long-Term Remote Sensing Data: Patterns, Causes and Implications

Wei Guo ^{1,2,*}, Hao He ¹, Xiaoting Li ¹  and Weigang Zeng ³¹ Department of Earth and Environmental Sciences, Xi'an Jiaotong University, Xi'an 710049, China² Institution of Global Environmental Change, Xi'an Jiaotong University, Xi'an 710049, China³ Key & Core Technology Innovation Institute of The Greater Bay Area, Guangzhou 510670, China

* Correspondence: williamguo@xjtu.edu.cn

Abstract: The Loess Plateau (LP) of China, which is the pilot region of the “Grain to Green Project” (GGP), has received worldwide attention due to its significant changes in the natural and social environment. Investigation of vegetation variations in response to climate change and human activities is vital for providing support for further ecological restoration planning. This paper aimed to monitor vegetation dynamics of the LP with trend comparisons of various vegetation types, disentangle the effects of climate variations and ecological programs on vegetation variations, and detect the consistency of vegetation variations. More specifically, vegetation dynamics during 1982–2015 were analyzed using the Global Inventory Modelling and Mapping System third-generation Normalized Difference Vegetation Index (GIMMS NDVI3g) data with the application of Breaks for Additive Season and Trend (BFAST) and Hurst Exponent. The results showed that: (1) Vegetation manifested a significant greening trend ($0.013 \text{ decade}^{-1}$, $p < 0.01$) in the LP during 1982–2015, and a breakpoint (BP) was detected in 1999, which was the beginning of the GGP. Interannual NDVI after the BP (ABP) showed more than 3.5 times greening rates compared to the NDVI before the BP (BBP). (2) Human activities dominated the vegetation variation (accounted for 59.46% of vegetation variation), among which reforestation and land-use change with steep slopes (i.e., $\geq 15^\circ$) lead to the greening after the GGP implementation. (3) Future trends should be noticed in the Forest Zone and Forest-Grass Zone, where the greening trends tend to slow down or even reverse in the southern LP. The long-term GIMMS NDVI3g time series and multiple geospatial analyses of this study might facilitate a better understanding of the mechanisms of vegetation variations for the assessment of the large restoration programs in fragile ecosystems.

Keywords: vegetation dynamics; climate change; human activities; Loess Plateau

Citation: Guo, W.; He, H.; Li, X.; Zeng, W. Greater Greening Trend in the Loess Plateau of China Inferred from Long-Term Remote Sensing Data: Patterns, Causes and Implications. *Forests* **2022**, *13*, 1630. <https://doi.org/10.3390/f13101630>

Academic Editor: Viacheslav I. Kharuk

Received: 7 September 2022

Accepted: 30 September 2022

Published: 5 October 2022

Publisher's Note: MDPI stays neutral with regard to jurisdictional claims in published maps and institutional affiliations.



Copyright: © 2022 by the authors. Licensee MDPI, Basel, Switzerland. This article is an open access article distributed under the terms and conditions of the Creative Commons Attribution (CC BY) license (<https://creativecommons.org/licenses/by/4.0/>).

1. Introduction

Vegetation is one of the most fundamental components of the terrestrial ecosystem, linking the matter and energy cycle among the hydrosphere, lithosphere, atmosphere, and biosphere due to its significant effects on carbon neutrality and climate change [1–3]. Hence, vegetation has been regarded as an irreplaceable part of maintaining the stability of regional and global ecosystems [4]. Meanwhile, over the past few decades, vegetation has shown widespread and tremendous variations under climate change and intensified anthropogenic intervention [5–7].

To address devastating land degradation and soil erosion, the Chinese government has launched a series of ecological engineering programs for environmental restoration and protection [8]. Many studies have shown that these programs have helped to increase vegetation cover and improve ecosystem services [9–11]. However, their environmental effects have not yet been systematically evaluated. Therefore, a long-term and comprehensive investigation of vegetation variation can help further study vegetation dynamics and assess

the effectiveness arising from those ecological projects for better ecosystem management and adaptation.

Remote sensing data provide broader ecological cues and make it possible to investigate vegetation variability and responses to climate change at large scales [12]. The satellite-based Normal Difference Vegetation Index (NDVI) has been most commonly used to detect vegetation variations, including key characteristics such as greenness, phenology, and productivity [13,14]. Many of the studies have been undertaken using long-term NDVI to analyze the effects of climate change on vegetation variations at different spatiotemporal scales, which reflected the availability of satellite-derived datasets at multiple resolutions in both space and time [15–17]. In particular, the Global Inventory Modelling and Mapping System third-generation Normalized Difference Vegetation Index (GIMMS NDVI3g) has been the longest-term available NDVI dataset [18]. This dataset has proved good quality and can provide more detailed vegetation dynamics without merging multi-source datasets to achieve data consistency.

Since the 1980s in the last century, widespread greening trends occurred globally [18,19]. Numerous examples of research have shown heterogeneity and mechanisms of greening, especially in the northern hemisphere [20–22]. Greening trends in northwestern China, especially in the fragile Loess Plateau (LP), have been widely concerned since severe water and soil erosion in the LP were caused by climate and land use changes over the past few decades [23]. In addition, LP is always the pilot region of an ecological restoration project in China. Approximately \$8.7 billion has been invested to convert the previous way of land use due to the implementation of the GGP in the year of 1999 [24]. Therefore, balancing the economic efficiency of eco-project and ecological goals is, thus, a great challenge [25].

Distinguishing the quantitative contribution of climate and human factors to vegetation variations is important for ecological restoration management. Although previous studies focused on detecting and assessing the effects of climate and non-climate factors on ecosystems [26,27], few detailed and systemic evaluations of responses of vegetation variations to climate change and anthropogenic intervention together in the LP. The contributions of factors to vegetation variations still remained unclear. In general, the causes of the vegetation dynamics are still not understood properly. This is due to multiple factors, including the lack of long-term monitoring and the absence of studies on driving forces and their contribution with multiple scales in space and time.

Global warming and excessive human activities in recent years have exacerbated a series of ecological issues (i.e., vegetation degradation, land desertification, soil erosion), leading to warming–drying trends with a higher frequency of droughts frequency in the LP [11,28]. Thus, accurate knowledge of vegetation variations and their responses to climate change and anthropogenic intervention could help in regulating ecological restoration planning and developing a sustainable ecosystem in the LP under projected climate change. A key question for this area is how the vegetation varies in the context of both climate change and anthropogenic intervention. Thus, the objectives of our research are to (1) detect the spatial-temporal patterns of vegetation variations and recognize significant greening and browning; (2) analyze the influences of climate changes on vegetation variations; (3) disentangle the influences of climate change and human activities on vegetation variations.

2. Materials and Methods

2.1. Study Area

The LP, located in the middle reach of the Yellow River (33°41′–41°16′ N, 100°52′–114°33′ E), with a total area of about 6.2×10^4 km², is the world's largest, most concentrated, and typical loess landform unit as well as a key area for severe water shortage and soil erosion in China. The mean annual temperature is 8.0 °C, and the annual precipitation is 439 mm. According to the zonal distribution of climate [29], the study region was divided into five zones from southeast to northwest as follows: Forest Zone, Forest-Grass Zone, Grass Zone, Grass-Desert Zone, and Desert Zone (Figure 1).

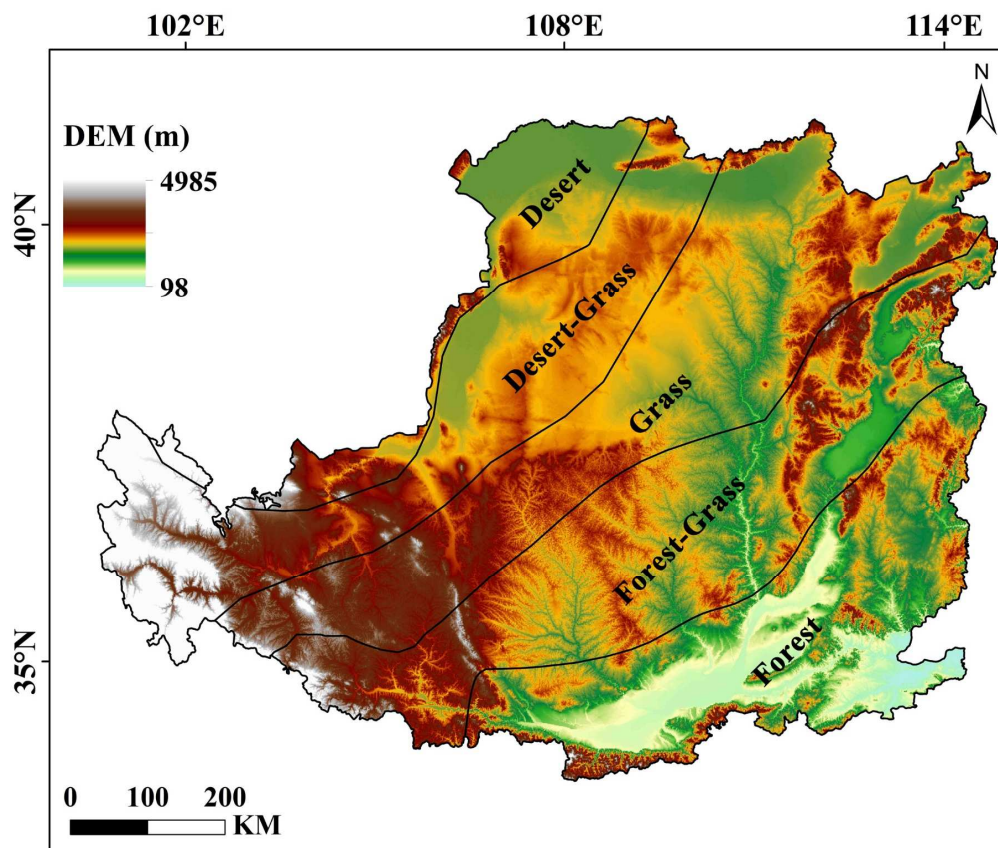


Figure 1. Map of the Loess Plateau (LP) and its bioclimatic zone division.

The region has sparse vegetation with a surface layer of wind-deposited fine-grained yellowish alluvium loess, which is particularly susceptible to erosion by water and heavy precipitation. Approximately 90% of the Yellow River's sediment is dominated by the characteristic of soil erosion in LP [30]. In addition, soil erosion causes the huge loss of vegetation nutrients, further reducing crop yield and vegetation primary productivity. Due to the fragile ecosystem and serious environmental problems, LP was selected as a GGP pilot area in 1999, focusing on returning steep cropland to forest and grassland. As a result, the spatiotemporal characteristics of land use have greatly changed.

2.2. Remote Sensing and GIS Data

The GIMMS NDVI3g data, provided by NASA's Global Inventory Monitoring and Modeling Studies (<https://ecocast.arc.nasa.gov/data/pub/gimms/>, accessed on 1 June 2021), with the longest period (from 1982 to 2015) at 1/12° spatial resolution and 15-day temporal resolution, was selected to monitor vegetation dynamics from 1982 to 2015 in this study. The features improved data quality by accounting for biases such as calibration loss, orbital drift, and volcanic eruptions, and it has been previously shown to represent the real response of vegetation to climate change [31]. The NDVI dataset of LP from 1982 to 2015 was obtained through format transformation, projection conversion, cropping, and outlier elimination based on the ArcGIS platform. The maximum synthesis method is used to acquire the monthly NDVI data, which can effectively eliminate the effect of errors caused by clouds and atmospheric and solar altitude angles [15].

Three-hourly gridded near-surface temperature, precipitation, and solar radiation data at 0.1° spatial resolution from the China Meteorological Forcing Dataset (CMFD), provided by the National Tibetan Plateau Data Center (<http://data.tpdc.ac.cn>, accessed on 15 August 2021), was used to identify the correlation with vegetation variations during 1982–2015. The mean temperature, accumulated precipitation, and accumulated solar radiation for monthly and annual were calculated using the ArcPy package in Python. Then, the climate data were resampled to $1/12^\circ$ spatial resolution to match the NDVI dataset.

The land use data were obtained from the China Resources and Environment Science Data Center with a spatial resolution of 1 km and a period from 2000 to 2015 in a 5-year interval. The land use types in the LP include cropland, forest, grassland, water, construction land, and unutilized land.

2.3. Geostatistical Analyses

2.3.1. Trend Analysis Methods

The Theil-Sen Median trend analysis (Sen) is a robust non-parametric trend statistical method. It characterizes the trend of the period by calculating the median slopes between any pair of combinations of the time series data, which can help reduce the influence of missing values or outliers [32].

$$S_{NDVI} = \text{Median}\left(\frac{NDVI_j - NDVI_i}{j - i}\right), \quad j > i \quad (1)$$

where S_{NDVI} is the NDVI trend; $NDVI_i$ and $NDVI_j$, respectively, are the NDVI value at years i and j . $S_{NDVI} > 0$ indicates that vegetation manifests a greening trend otherwise manifests a browning trend.

The Mann-Kendall statistical test was applied to test the significance of the NDVI trend. It is a non-parametric test method with superiorities in effectively eliminating the effect of outliers and not requiring the sample to obey a specific distribution [32]. The statistic Z can be calculated with Equation (2):

$$Z = \begin{cases} \frac{S-1}{\sqrt{\text{Var}(S)}} & , S > 0 \\ 0 & , S = 0 \\ \frac{S+1}{\sqrt{\text{Var}(S)}} & , S < 0 \end{cases} \quad (2)$$

where the statistic S is the size relationship of all $n(n-1)/2$ pair combinations and the $\text{Var}(S)$ is its variance. When the size of the sample is greater than 10, S approximates standard normal distribution and the $\text{Var}(S)$ is estimated as follows:

$$\text{Var}(S) = \frac{n(n-1)(2n+5) - \sum_{i=1}^m t_i(t_i-1)(2t_i+5)}{18} \quad (3)$$

where m is the number of repeated datasets in the sequence; t_i is the number of the i th set of repeated data; n is the sample size.

At the given significance level α , the threshold of the normal distribution is $Z_{1-\alpha/2}$. If $|Z| > Z_{1-\alpha/2}$, the NDVI trend is significant on the level α . In this study, we choose $\alpha = 0.05$ ($Z = \pm 1.96$) and $\alpha = 0.01$ ($Z = \pm 2.58$) to test the significance of gridded NDVI trend.

2.3.2. Hurst Exponent

The Hurst exponent, proposed by Hurst (1951), is widely used to distinguish the sustainability of long-term time series. The Hurst exponent can be calculated with Equation (4) [28]:

$$\frac{R(\tau)}{S(\tau)} = (c\tau)^H \quad (4)$$

where $R(\tau)$ is the extreme deviation sequence; $S(\tau)$ is the standard deviation sequence; H is the Hurst exponent ranging from 0 to 1. When $H < 0.5$, it means that the trend of NDVI series in the future would be opposite to the present; when $H = 0.5$, it means that the trend of NDVI series in the future would be independent of the study period; when $H > 0.5$, it means that the trend of NDVI series in the future would continue with the present trend.

2.3.3. Breaks for Additive Season and Trend (BFAST)

BFAST is a method to quantify the trends and breakpoints (BPs) of time series, which typically have a periodic pattern [33]. It is an additive decomposition model that iteratively fits a piecewise linear trend and seasonal model of the time series [34] and detects and characterizes BPs in the trend and seasonal components according to specific methods. The general form of the model is [35–37]:

$$Y_t = T_t + S_t + e_t, \quad t = 1, 2, \dots, n \quad (5)$$

where Y_t is the NDVI value at time t ; T_t is the trend component; S_t is the seasonal component; e_t is the remainder component, which is the variation component other than the trend component and seasonal component. The intercept and slope of the trend component model are used to derive the magnitude and direction of abrupt change. This study was based on the BFAST package in R x64 4.0.2 and RStudio (<http://www.r-project.org/>, accessed on 15 September 2021) to detect the dynamic change of vegetation.

2.3.4. Quantitative Contribution Method

The Pearson correlation method was applied to characterize the responses of vegetation to climate change. Furthermore, since vegetation variations have been considered a function of climate variability and anthropogenic activities, the contributions of climatic and anthropogenic factors to vegetation variations can be effectively quantified by the Residual trend method [14]. Specifically, we split the NDVI time series into subperiods t_1 (climatic domination) and subperiods t_2 (anthropogenic domination). The predicted NDVI value was generated by climate over subperiod t_2 based on the regression equation of NDVI response to climate constructed over subperiod t_1 . Then the residual of the simulated and observed NDVI was the contributions of each factor [26].

3. Results

3.1. Temporal Variability of NDVI Trend at Regional Scales

During the study period, NDVI values highlighted some temporal fluctuations in greenness across the whole plateau from 1982–2015. Vegetation activity in the LP generally increased with a statistically significant overall uptrend at the rate of $0.013 \text{ decade}^{-1}$ ($p < 0.01$) through linear regression analysis (Figure 2a). In detail, the annual average NDVI of the whole plateau showed a substantial decline in the year 1999, after then the upward trend continued reaching maximums in 2013.

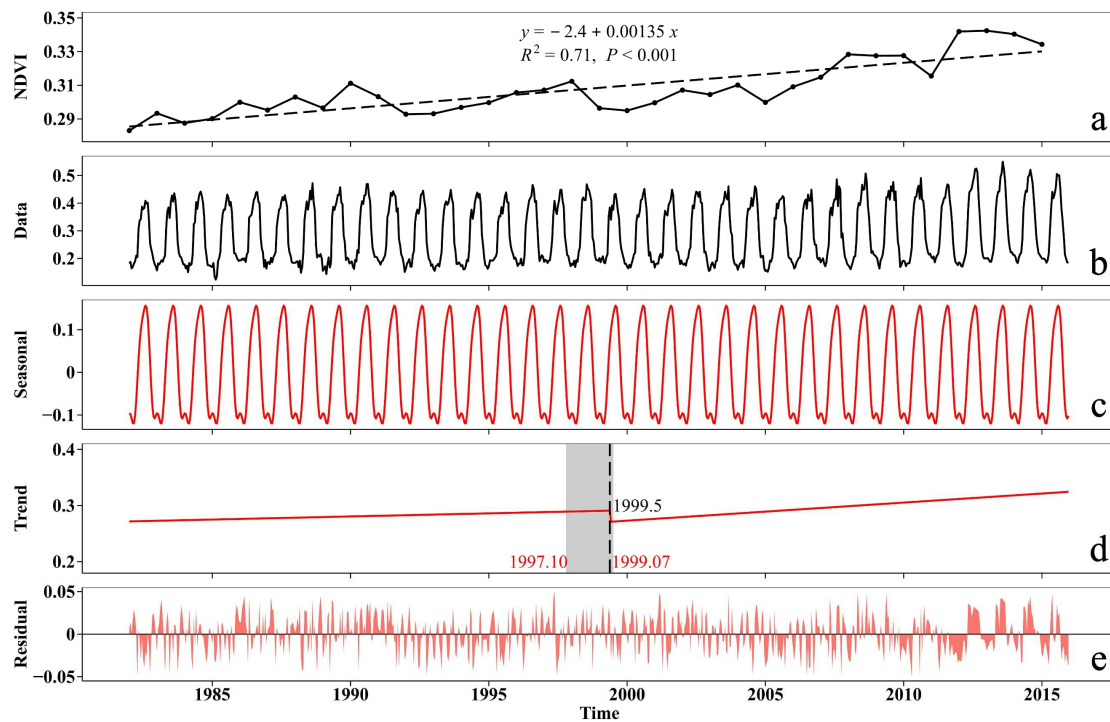


Figure 2. (a) Inter-annual variability of regionally averaged NDVI in the LP and (b) original NDVI time series, (c) seasonal, (d) trend, and (e) residual components of the NDVI time series decomposed by Breaks for Additive Season and Trend (BFAST). The breakpoint (BP) are black dashed lines and the confidence interval on the 0.05 level is grey-inked in the trend component.

In order to fit piecewise linear trends and detect vegetation abrupt changes, this study employed the BFAST method to monitor vegetation dynamics. The results indicated that no seasonal or phenological changes have been identified in the LP during 1982–2015 given the consistent seasonal components of the NDVI time series in the past three decades (Figure 2c). There was a significant BP in the NDVI trend components (Figure 2d). The BP of NDVI across the plateau occurred mainly in 1999. In addition, 1999 was also the starting year of the GGP implementation. Therefore, we treated the year 1999 as the BP year and split the study periods into the before BP (BBP, 1982–1999) and after BP (ABP, 2000–2015).

3.2. NDVI Variability Comparison

3.2.1. NDVI Change in Regional Scales

In general, vegetation on the whole plateau showed increasing trends of both BBP and ABP among interannual and intra-annual scales. More importantly, the increasing rate of NDVI in ABP was much higher than that of NDVI in BBP on all time scales. Specifically, in BBP, NDVI increased at a rate of $0.009 \text{ decade}^{-1}$, $0.013 \text{ decade}^{-1}$, $0.008 \text{ decade}^{-1}$, and $0.009 \text{ decade}^{-1}$ in the interannual, spring, summer, and autumn periods, respectively (Figure 3). However, NDVI increased sharply in ABP at the rate of $0.031 \text{ decade}^{-1}$, $0.027 \text{ decade}^{-1}$, $0.055 \text{ decade}^{-1}$, and $0.028 \text{ decade}^{-1}$ in the interannual, spring, summer, and autumn ($p < 0.01$), approximately 3.5, 2, 7, and 3 times of the BBP changes.

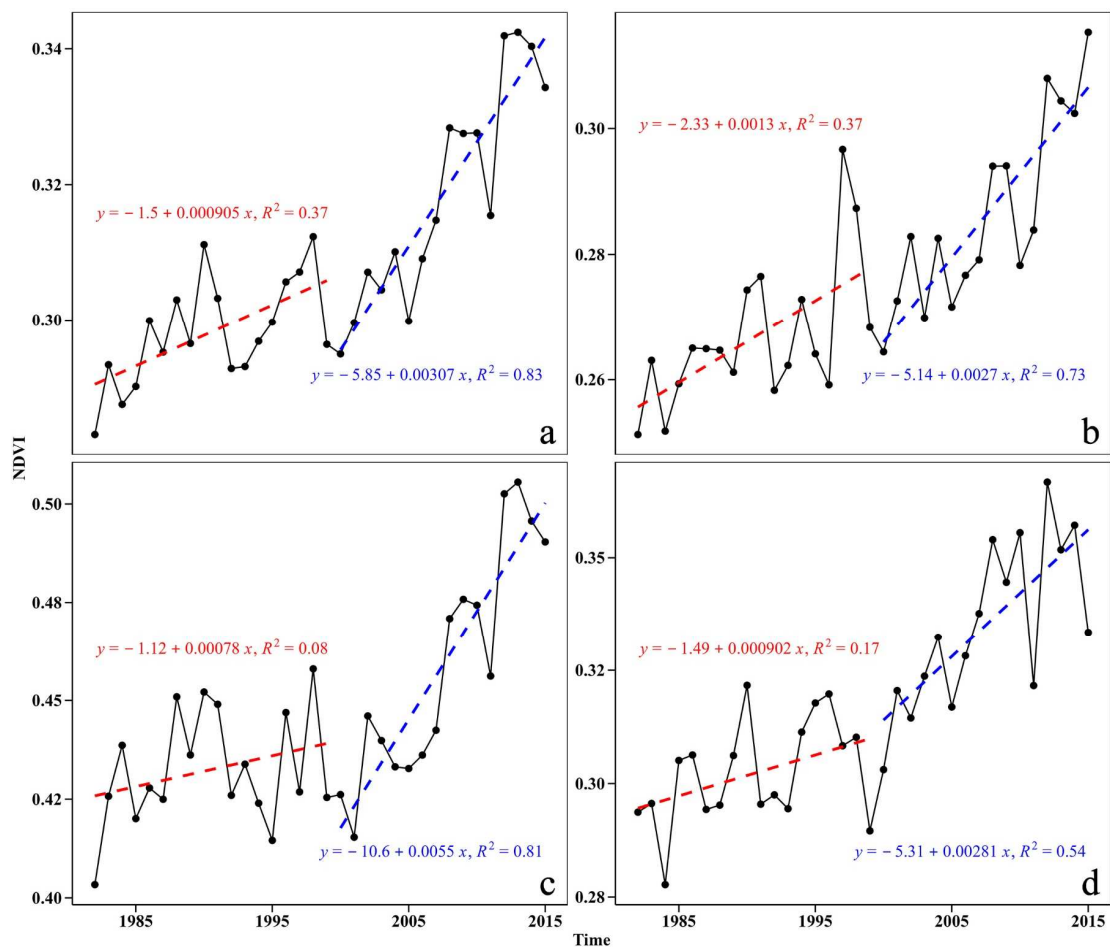


Figure 3. Interannual variations in NDVI of (a) interannual scale, (b) spring, (c) summer, and (d) autumn in the LP from 1982 to 2015. The lines in red and blue represent the NDVI trend before the BP (BBP, 1982–1999) and after the BP (ABP, 2000–2015), respectively.

The temporal trend of NDVI in BBP and ABP indicated an overall increasing trend in different periods across the LP (Figure 4a–c). From 1982 to 2015, the vegetation was characterized by a significant increase in the NDVI which covered approximately 95.1% of the plateau, whereas only 4.9% of the vegetation experienced negative trends (Figure 4a). In the area of vegetation improvement, the extremely significantly ($p < 0.01$) increased area accounted for 73.2%, mainly distributed in forest and grass areas. In the vegetation degradation area, 3.7% of the area was reduced ($p < 0.01$), and the significantly reduced areas accounted for 1.2%, which are mainly distributed in densely populated areas such as the urban areas in the northwest of the LP.

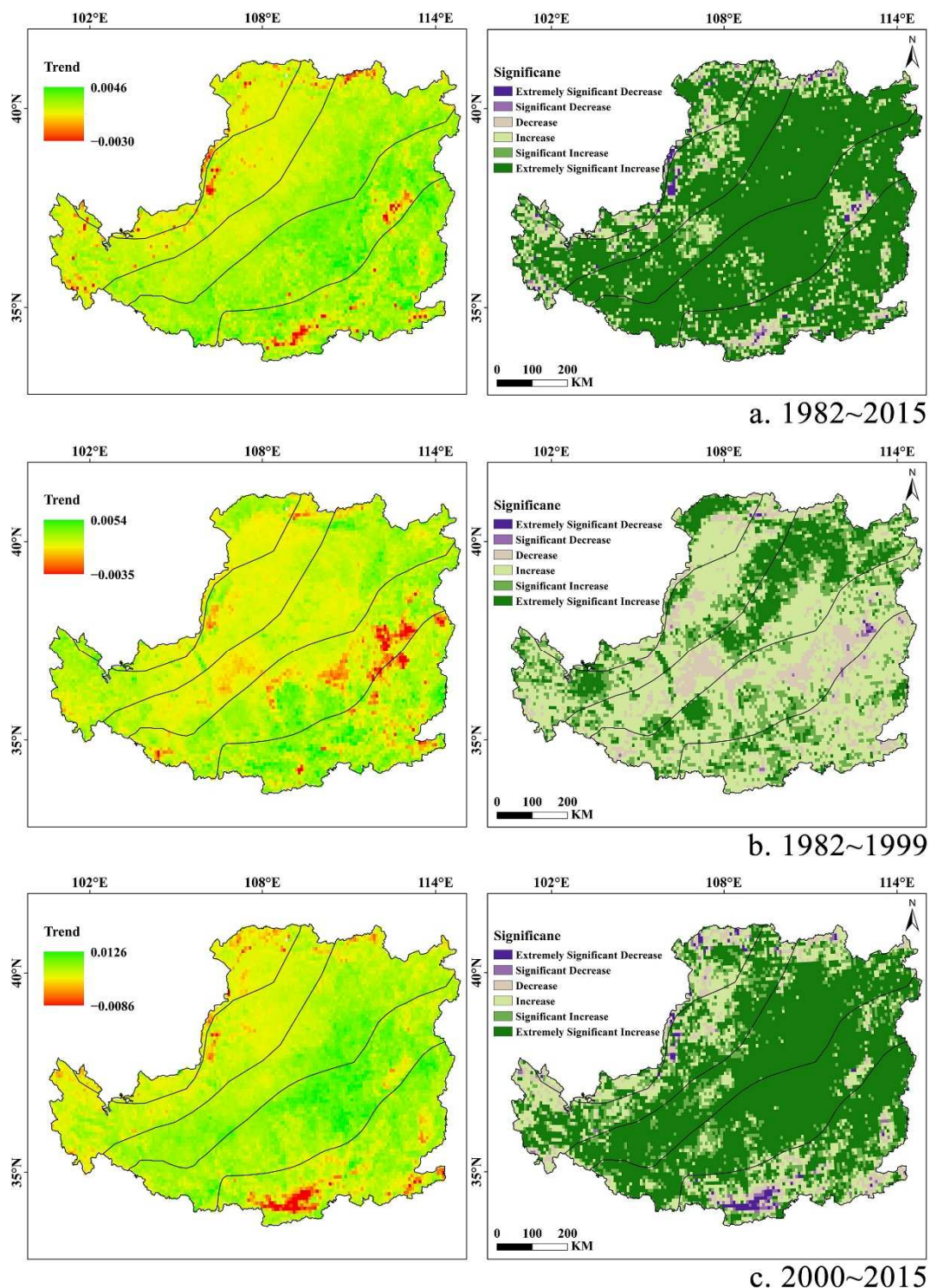


Figure 4. Spatial patterns of the NDVI changes and corresponding p values for (a) 1982–2015; (b) 1982–1999 (BBP); (c) 2000–2015 (ABP).

The averaged trend of NDVI change in BBP was $0.0094 \text{ decade}^{-1}$ spatially, and the areas showing increasing and decreasing trends accounted for 88.6% and 11.4%, respectively (Figure 4b). However, the trend of NDVI change in ABP was $0.031 \text{ decade}^{-1}$ spatially, nearly 3 times of the BBP changes. The proportion of areas with an extremely significant increasing trend rose obviously from 19.2% in BBP to 60.3% in ABP, and they were detected mainly in the central LP where the GGP occurred (Figure 4b,c).

3.2.2. NDVI Change among Bioclimatic Zones

Five bioclimatic zones had the same increasing temporal trend as the LP (whole region), among which the change rate of the Forest-Graass Zone and Grass Zone in ABP were even greater than those of LP, reaching $0.048 \text{ decade}^{-1}$ and $0.037 \text{ decade}^{-1}$, respectively (Figure 5a). In addition, the highest proportion of areas with significantly increasing trends was found in Forest-Graass Zone (90.21%) and Grass Zone (89.08%) NDVI in ABP, and the proportion increased sharply compared to the NDVI trends in BBP (Figure 5b). The results were consistent with Li et al. [38] and Fu et al. [39], indicating that the GGP had achieved an overall restoration of forests and grasslands, which showed an extensive spatial distribution in the LP as shown in Figure 4. The restored forests and grasslands were mostly located in the central Loess hilly and gully area. Specifically, the Forest-Graass Zone achieved the highest restoration ($15.57 \times 10^4 \text{ km}^2$), followed by the Grass Zone ($16.82 \times 10^4 \text{ km}^2$) owing to the suitable natural conditions.

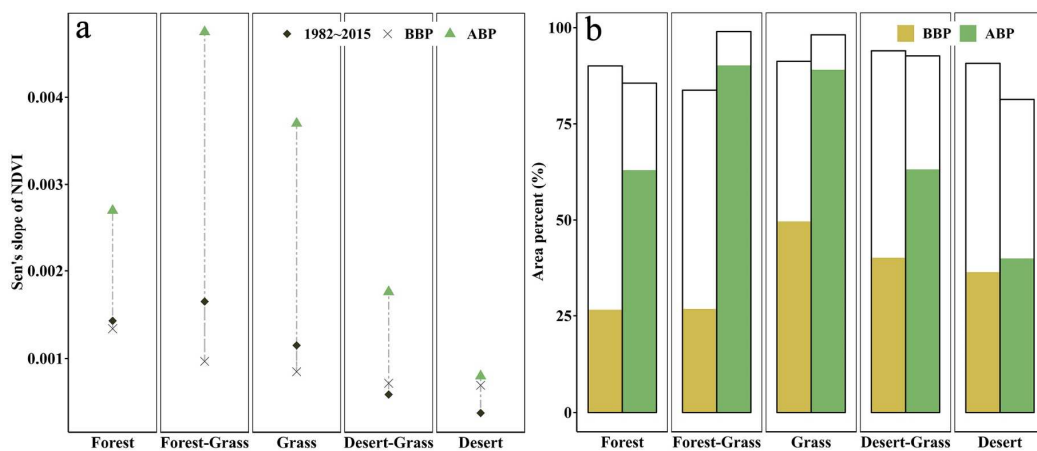


Figure 5. Trends of NDVI variation in five bioclimatic zones over different periods. (a) Average changing rate; (b) Percentage of the greening area with significant ($p < 0.05$) variations of NDVI.

3.2.3. The Sustainability of NDVI Change

The sustainability of vegetation dynamics trends was assessed by using the Hurst method. As shown in Figure 6, the results were divided into 4 categories: strong persistent (0.6–1), weak persistent (0.5–0.6), weak anti-persistent (0.4–0.5), and strong anti-persistent (0–0.4). The Hurst exponent of the LP is 0.47 on average. The sustainable area, accounted for 39.46%, mainly concentrated in the Grass Zone of the central LP. The area with anti-persistent trends accounted for 60.54% and is mainly distributed in the cities where human activities are intensive.

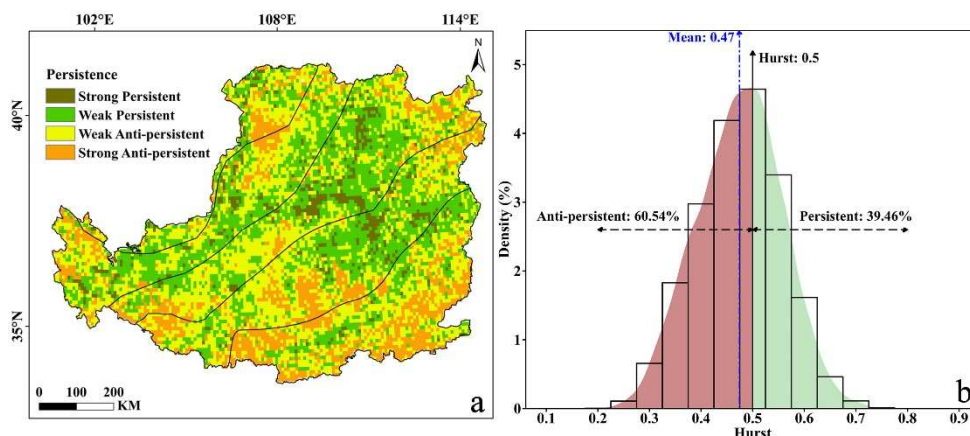


Figure 6. (a) Hurst exponent spatial distribution and (b) frequency distribution histogram.

3.3. Vegetation Change and Climatic Factors

3.3.1. Climatic Variability Trends from 1982–2015

NDVI and climatic factors showed similar spatial patterns. An increased tendency of NDVI extended horizontally from northwest to southeast, which was strongly related to the increasing tendency in temperature, precipitation, and solar radiation (Figure 7). These suggested that the spatial patterns in NDVI are closely related to climatic factors.

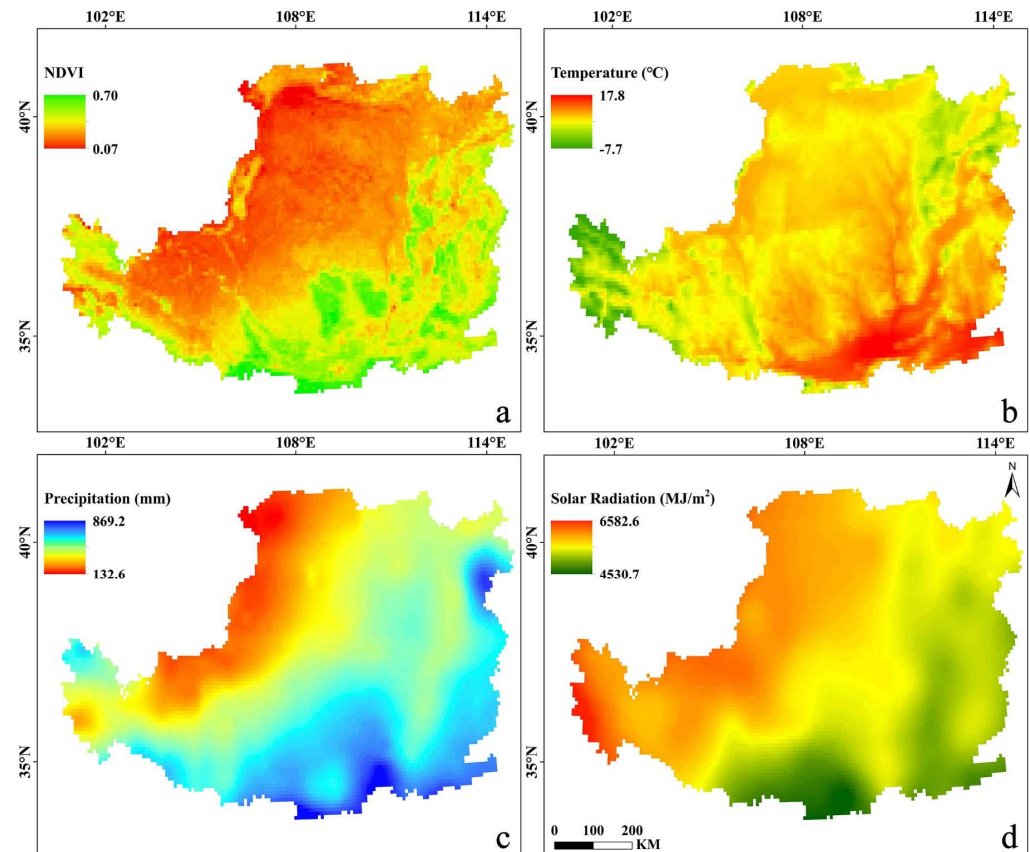


Figure 7. Spatial patterns of 34 years of mean (a) NDVI, (b) temperature, (c) precipitation, and (d) solar radiation in the LP.

The climate of the LP has changed over the past few decades. The temperature in the LP showed an increasing overall trend ($0.41\text{ }^{\circ}\text{C decade}^{-1}$) (Figure 8b). To be precise, it increased in the years before 1999 ($0.63\text{ }^{\circ}\text{C decade}^{-1}$) then increased at a much gentler rate ($0.13\text{ }^{\circ}\text{C decade}^{-1}$) afterwards. The precipitation also showed an increasing trend ($20.2\text{ mm decade}^{-1}$) in the recent 34 years, with a smaller ABP increasing rate ($11.1\text{ mm decade}^{-1}$) (Figure 8c). Unlike the temperature and precipitation trend, radiation showed a decreasing overall trend change during 1982–2015. Specifically, radiation showed a greater decreasing trend ($-27.8\text{ MJ decade}^{-1}$) before 1999 but a slightly decreasing trend afterwards (Figure 8d). Overall, the change of rate of climatic factors in the LP was greater in BBP than in ABP.

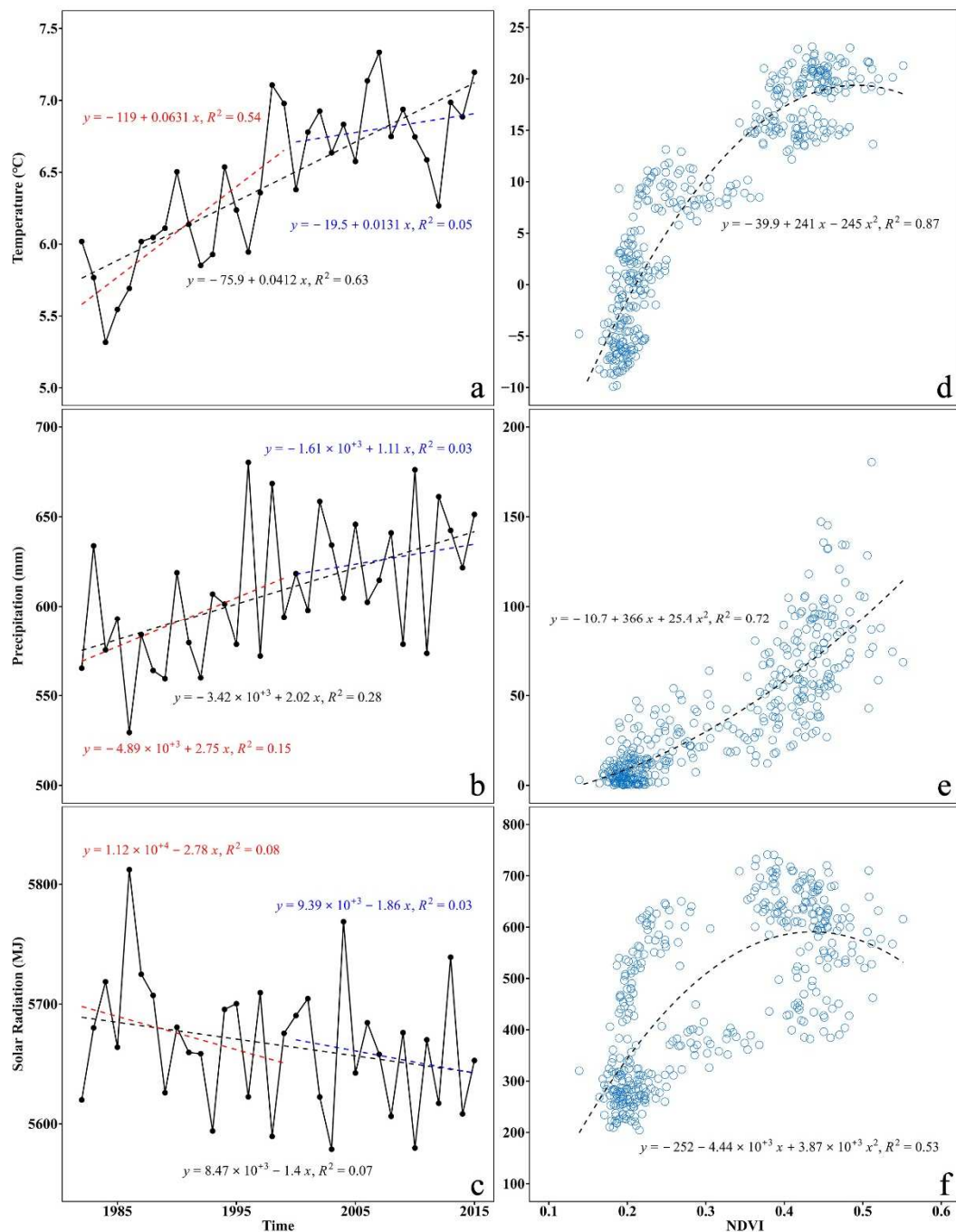


Figure 8. Trends of climatic factors variation and its relations to NDVI changes. The left panel represents interannual variations in (a) temperature, (b) precipitation, and (c) solar radiation over different periods. The right panel represents the relationship between NDVI and (d) temperature, (e) precipitation, and (f) solar radiation.

3.3.2. Correlation between NDVI and Climatic Factors

The correlations between NDVI and climatic factors were spatially varied (Figure 9). The correlations between NDVI and temperature were positive in 90.22% of areas whereas only 9.78% of urban areas had a negative NDVI-temperature relationship. For the relationship of NDVI-precipitation, 84.54% of the regions showed positive correlation, mostly distributed in the central and north of the LP, whereas negative correlations mainly occurred in the south of the LP accounting for 18.45%. The correlation between NDVI and

radiation was mostly positive in the south and negative in the northwest and east of the LP from 1982 to 2015, and the area fractions were 37.87% and 62.13%, respectively.

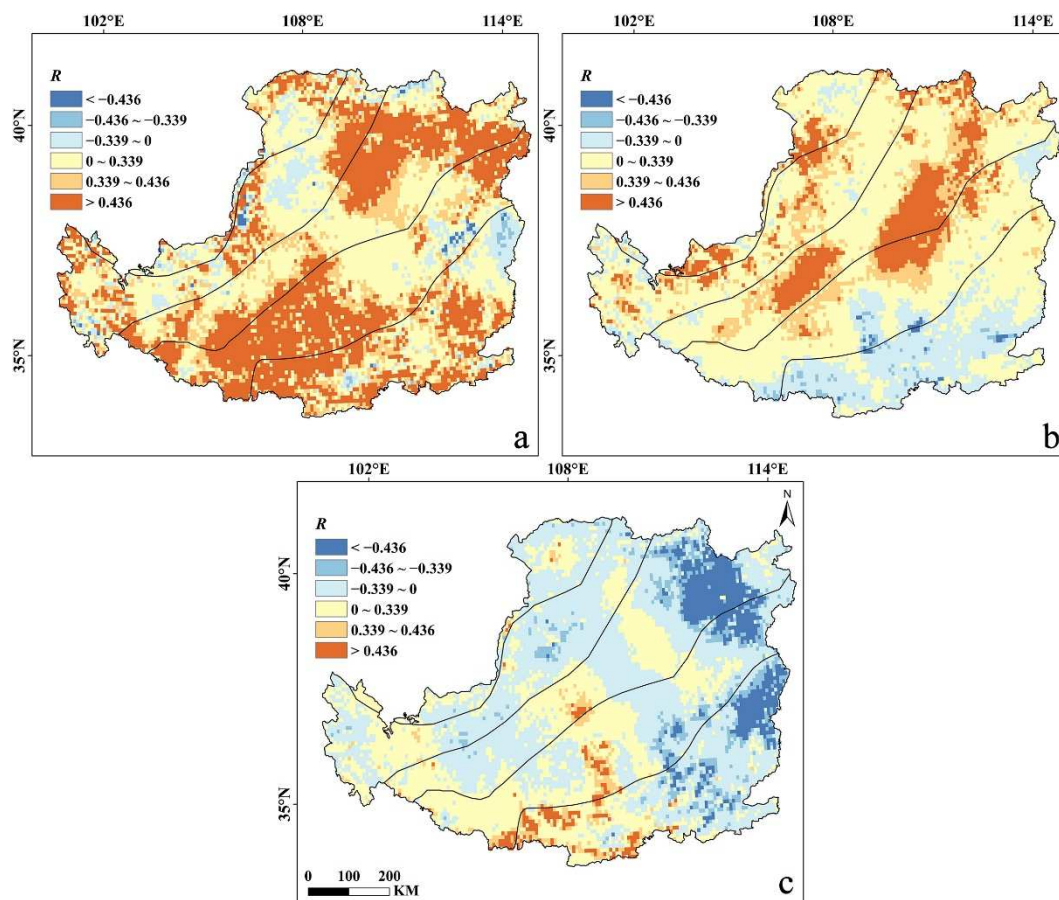


Figure 9. Spatial distributions of response relationships between NDVI and (a) temperature, (b) precipitation, and (c) solar radiation. The absolute values of R greater than 0.339 represent significant correlations ($p < 0.05$).

However, the NDVI-climate relationship varied in different periods (Table 1). Specifically, over BBP, the correlation coefficients of temperature and precipitation versus NDVI were 0.58 and 0.41, respectively, while they were 0.16 and 0.30 for ABP. The correlation coefficients between radiation and NDVI changed from -0.01 for BBP to -0.18 for ABP. Furthermore, compared with BBP, the change rate of NDVI over ABP are 3.5 times of those in BBP and significantly increased during ABP. These results suggested that climate change dominated the NDVI variations in BBP, whereas it was more subject to other factors (e.g., human activities) in ABP. Therefore, we speculated that recent large-scale ecological restoration, especially the GGP project, dominated vegetation coverage increase.

Table 1. Correlation between NDVI and climate factors.

Climate Factors	Correlation Coefficients		
	1982–2015	BBP	ABP
Temperature	0.61 **	0.58 *	0.16
Precipitation	0.50 **	0.41	0.30
Solar Radiation	-0.19	-0.01	-0.18

Note: * and ** represent significance at $p < 0.05$ and $p < 0.01$.

3.3.3. Contribution of Ecological Restoration Project

Evidence from land-use change in the LP showed that the area of croplands was decreasing while the area of forests was increasing after 2000 as the increased impacts of human activities (Figure 10b,c). Overall, vegetation coverage in terms of NDVI was the highest for forests, intermediate for grassland, and lowest for shrubs and sparse vegetation. In ABP, the area of croplands and grasslands decreased by 5620.03 km² and 1776.27 km², while the area of forests and construction land increased by 2608.23 km² and 5169.76 km² (Figure 10a). In addition, the decrease in croplands was greater at higher elevations and steeper slopes (15–25°), where forests tended to substitute croplands (Figure 11). Therefore, the NDVI increase for forests and grasslands was probably due to the sustainable afforestation in higher and steeper regions.

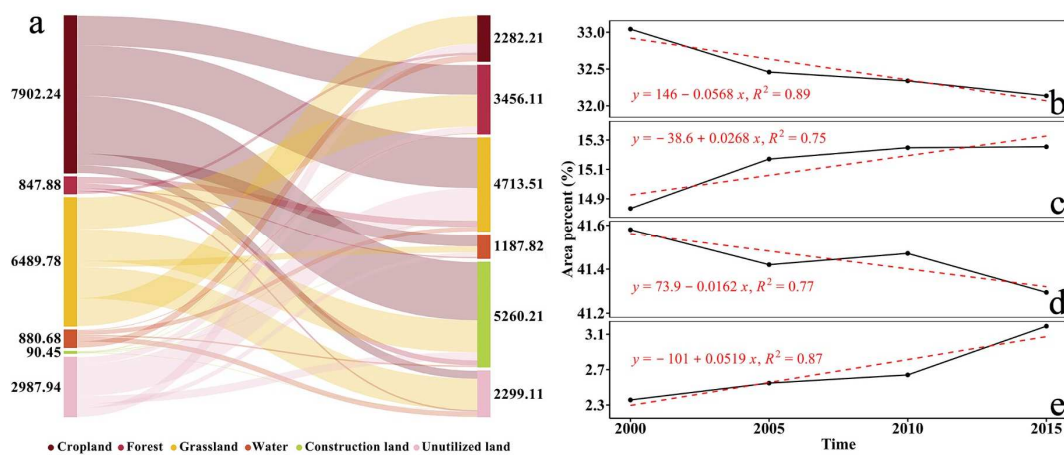


Figure 10. Land-use change of the LP in ABP: (a) Land use transition among different land types, and changes of (b) croplands, (c) forests, (d) grasslands, and (e) construction land.

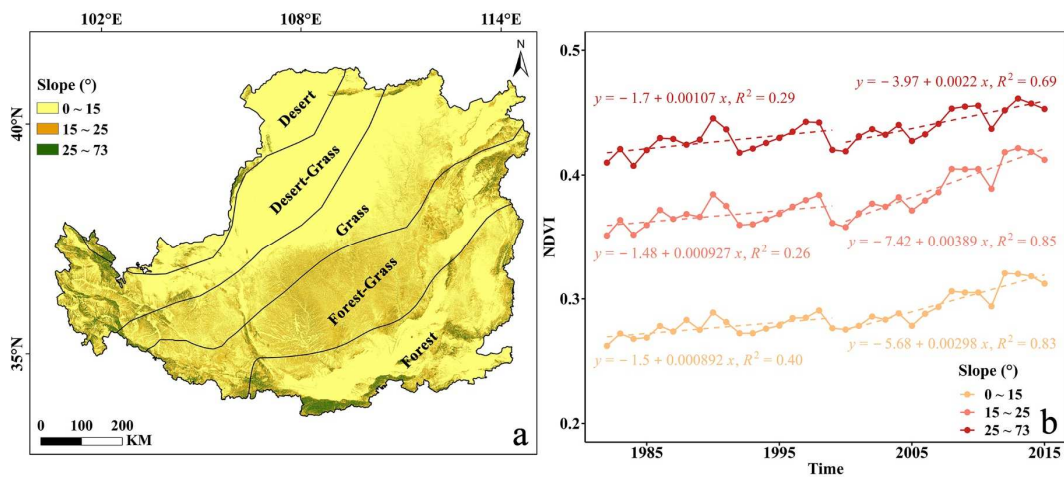


Figure 11. (a) Slope map of the LP, and (b) NDVI variation trends in different slopes.

The impact of human activities on vegetation change in ABP was more important than climate change, and the contributions of human activities and climate change accounted for 59.46% and 40.54%, respectively (Table 2). In the five bioclimatic zones, human activities had a greater impact on vegetation in Forest Zone, Forest-Grass Zone, and Grass Zone, whereas the characteristic was opposite in the Desert-Grass Zone and Desert Zone. More specifically, the vegetation changes in Desert-Grass Zone and Desert Zone, where the soil foundation condition is severe, were affected by climate change, accounting for 51.32% and 55.88%, respectively. However, human activities in the remaining bioclimatic zones were

the main factor leading to vegetation changes, with contributions exceeding 50%, reaching the top in the Grass (77.14%), and this was obviously due to the impact of the GGP in the forest and grass area with higher vegetation coverage.

Table 2. The contribution of climate driving forces and human activities for vegetation variations.

Region	NDVI Changes			Contribution (%)	
	BBP	ABP	Total	Climate	Human
LP	0.2982	0.3186	0.0204	40.54	59.46
Forest	0.4428	0.4658	0.0230	41.76	58.24
Forest-Grass	0.3677	0.3972	0.0295	45.73	54.27
Grass	0.2309	0.2537	0.0228	28.86	77.14
Desert-Grass	0.2130	0.2232	0.0102	51.32	48.68
Desert	0.1639	0.1706	0.0067	55.88	44.12

Note: The monthly temperature and precipitation were selected as climatic factors to construct a regression equation due to their higher significant correlation with the NDVI (Table 1).

4. Discussion

4.1. Time Series Detection

Vegetation variations are complex and are driven by multiple eco-physiological processes and exert strong feedback on the Earth's systems. Therefore, continuous monitoring plays an irreplaceable role in global change research and ecological protection. Since the 1980s, vegetated lands have experienced widespread change. Strong evidence of vegetation "greening" at various scales was provided with the development of remote sensing technologies [15,19,20,40]. To understand the vegetation dynamics and potentially abrupt changes from 1982–2015 in the LP, the present study analyzed the spatiotemporal variability of vegetation using the long time series of satellite-derived GIMMS NDVI3g datasets.

Warming-induced increases in NDVI have been observed in most Northern Hemisphere regions, suggesting a persistent and gradual change in interannual time scales [41,42]. However, there has been little discussion about the abrupt change in the NDVI time series. The latter is considered essential for understanding and predicting ecosystem responses to changing climates. Therefore, the relationship between vegetation and climate change must be investigated at multiple spatiotemporal scales, including seasonal, interannual, and interdecadal timescales, as well as from regional to bioclimatic zone and pixel-level in space scales and their combinations.

The BFAST method was found to be helpful for detecting features of vegetation dynamics [37]. With the establishment of a long-term dynamic detection and regular assessment system especially for the regions with vulnerable ecosystems, the policy makers can properly adjust and prioritize restoration measures specifically tailored to the local changing environment. And our findings showed that the GIMMS NDVI3g time series and multiple time scales analysis might facilitate a better understanding of the mechanisms of NDVI variations for ongoing ecosystem monitoring and assessment of the vegetation dynamics in fragile ecosystems.

4.2. Vegetation Change Causes

Hydrothermal conditions in the climatic environment are the primary natural factor controlling vegetation growth. Vegetation dynamics and their correlations with climate change constitute an essential dimension of global change research. Previous studies have shown that climatic factors such as rainfall, air temperature, and solar radiation are the main factors affecting vegetation greenness and production in arid and semi-arid regions [7,43]. Meanwhile, the impact of changes in human activities on vegetation dynamics is well recognized in extensive research [44,45]. Our results also indicated that vegetation change could not be fully explained by climatic factors in the LP, especially after the BP year of 1999. Evidence has shown that the ecological restoration projects have significantly increased vegetation cover, despite the relative warm-dry climate condition

across the whole plateau after the BP year of 1999. Furthermore, the LUCC changes mainly demonstrated that croplands contraction and forests expansion during 2000–2015 in the LP, which was consistent with the implementation of GGP. In addition, extremely significant ($R^2 > 0.661$) accelerated greening after 2000 mainly occurred in the central plateau with steep slopes (i.e., $\geq 15^\circ$), which demonstrated returning sloping croplands to forests or grasslands to restore vegetation cover according to the white paper, “Twenty Years of Converting Farmland to Forest and Grass in China”.

Quantitatively distinguishing the relative impact of climate change and human activity is vital for understanding vegetation dynamics [46]. Thus, we explored the relationship between climate and NDVI in BBP to reconstruct NDVI in ABP. The well-developed equations between climatic factors and NDVI suggested that the method performed well in reconstructing vegetation under natural conditions. The results showed that human activities, such as reforestation and land-use change were the major drivers, even greater than climatic factors in ABP after the GGP implementation. This means the vegetation greening trend could be attributed to the implementation of the GGP. More importantly, the quantitative contributions of climate and human activities were 40.54% and 59.46%, respectively. However, human activities imposed both positive (e.g., afforestation) and negative (e.g., forest destruction and urbanization) effects. These findings have shed light on the mechanics of NDVI variations in the periods before and after the GGP implementation.

4.3. Ecological Management Implications

Long-term trends of vegetation variations can not only reveal the current process but also indicate potential changing directions of ecosystems. And the latter was particularly important for the ecological program planning and implementation. Our results showed that grasslands are more sustainable than forests, shrub lands, and sparsely vegetated areas. The strong anti-persistent trend in the Forest Zone and Forest-Grass Zone of the southern LP should be noticed, which suggests a browning trend in the coming years. This should be carefully considered in natural resource management.

The major reason behind this reversing trend may be attributed to shortages in the water supply. Water is crucial to sustain the greening. The LP is viewed as a typical arid and semi-arid area in northern China. Ecological restoration projects may result in potential conflicts between water use for the ecological environment and socioeconomic development in those water-limited regions [47]. The water demand from rapid urbanization and agricultural and industrial development has increased sharply over the same time as new planting areas have substantially expanded [25]. In such a situation, a restoration project without consideration of hydrological balance will aggravate the ecological conflict, especially in water-limited areas. For example, the newly planted trees have been found to consume excessive soil water, which in turn greatly affects the water balance of the entire plateau. However, it is worth noting that the survival rate of the planting of a large amount of non-native species is less than 20% based on the China Forest Resource Report [48,49]. Therefore, for the ecologically sustainable development of the LP, a large-scale restoration program should select suitable vegetation types to local conditions. In the future, determining the regional threshold of vegetation cover is a prerequisite for realizing large-scale revegetation projects are socially and ecologically sustainable.

5. Conclusions

The present study analyzed the vegetation dynamics and their relationships with climatic factors and anthropogenic effects in the LP from 1982–2015. Vegetation observed by GIMMS NDVI3g showed a greening trend in the LP over the past three decades. The greening vegetation effectively improved the regional ecosystem. In addition, abrupt change in the decomposed NDVI time series was found in the year 1999: BBP, the uptrend of NDVI was restrained into a relatively positive trend ($0.009 \text{ decade}^{-1}$, $p < 0.01$); ABP; however, NDVI exhibited a sharper uptrend with a rate of $0.031 \text{ decade}^{-1}$ ($p < 0.01$). Results showed that vegetation greenness was associated with climatic gradients across the platform and

both were spatially varied with great heterogeneity. Accelerated greening after BP year of indicated vegetation variation was strongly linked with the GGP implementation. Specifically, the quantitative contributions of climate and human activities were 40.54% and 59.46%, respectively. In addition, climate change and human intensity in the LP will exacerbate the water conflict between humans and ecosystems. Hence, ecological restoration projects should take into account the regional water cycle and balance. More importantly, long-term monitoring and periodic evaluation should be established in the large-scale revegetation programs to provide useful information to the plan in a fragile ecosystem.

Author Contributions: Conceptualization, W.G.; methodology, W.G., H.H. and X.L.; software, H.H. and X.L.; validation, W.G. and H.H.; formal analysis, W.G. and H.H.; investigation, W.G. and H.H.; resources, W.G.; data curation, H.H. and W.G.; writing—original draft preparation, W.G. and X.L.; writing—review and editing, W.G., H.H., X.L. and W.Z.; visualization, H.H.; supervision, W.G., X.L. and W.Z.; project administration, W.G.; funding acquisition, W.G. All authors have read and agreed to the published version of the manuscript.

Funding: This study was supported by the Strategic Priority Research Program of Chinese Academy of Sciences (XDB40020200), the National Natural Science Foundation of China (42071124), the Carbon Neutrality Monitoring Decision Application System (ZY-2021-005), the State Key Laboratory of Loess and Quaternary Geology (SKLLQG1809), and the Fundamental Research Funds for the Central Universities (XZY012019008).

Data Availability Statement: Publicly available datasets were used in this study. The GIMMS NVDI3g products were acquired from the NASA's Global Inventory Monitoring and Modeling Studies (<https://ecocast.arc.nasa.gov/data/pub/gimms/> (accessed on 1 June 2021)). The China Meteorological Forcing datasets were publicly available from the National Tibetan Plateau Data Center (<http://data.tpdc.ac.cn> (accessed on 15 August 2021)). The land use data were available from the China Resources and Environment Science Data Center (<https://www.resdc.cn> (accessed on 30 September 2021)).

Conflicts of Interest: The authors declare no conflict of interest.

References

1. Hua, W.; Chen, H.; Zhou, L.; Xie, Z.; Qin, M.; Li, X.; Ma, H.; Huang, Q.; Sun, S. Observational Quantification of Climatic and Human Influences on Vegetation Greening in China. *Remote Sens.* **2017**, *9*, 425. [[CrossRef](#)]
2. Wang, C.; Wang, S.; Fu, B.; Lü, Y.; Liu, Y.; Wu, X. Integrating Vegetation Suitability in Sustainable Revegetation for the Loess Plateau, China. *Sci. Total Environ.* **2021**, *759*, 143572. [[CrossRef](#)] [[PubMed](#)]
3. Qiu, L.; Wu, Y.; Yu, M.; Shi, Z.; Yin, X.; Song, Y.; Sun, K. Contributions of Vegetation Restoration and Climate Change to Spatiotemporal Variation in the Energy Budget in the Loess Plateau of China. *Ecol. Indic.* **2021**, *127*, 107780. [[CrossRef](#)]
4. Gu, Z.; Duan, X.; Shi, Y.; Li, Y.; Pan, X. Spatiotemporal Variation in Vegetation Coverage and Its Response to Climatic Factors in the Red River Basin, China. *Ecol. Indic.* **2018**, *93*, 54–64. [[CrossRef](#)]
5. Chen, A.; He, B.; Wang, H.; Huang, L.; Zhu, Y.; Lv, A. Notable Shifting in the Responses of Vegetation Activity to Climate Change in China. *Phys. Chem. Earth Parts A/B/C* **2015**, *87–88*, 60–66. [[CrossRef](#)]
6. Chu, H.; Venevsky, S.; Wu, C.; Wang, M. NDVI-Based Vegetation Dynamics and Its Response to Climate Changes at Amur-Heilongjiang River Basin from 1982 to 2015. *Sci. Total Environ.* **2019**, *650*, 2051–2062. [[CrossRef](#)] [[PubMed](#)]
7. Xu, W.; Liu, H.; Zhang, Q.; Liu, P. Response of Vegetation Ecosystem to Climate Change Based on Remote Sensing and Information Entropy: A Case Study in the Arid Inland River Basin of China. *Environ. Earth Sci.* **2021**, *80*, 132. [[CrossRef](#)]
8. Lu, F.; Hu, H.; Sun, W.; Zhu, J.; Liu, G.; Zhou, W.; Zhang, Q.; Shi, P.; Liu, X.; Wu, X.; et al. Effects of National Ecological Restoration Projects on Carbon Sequestration in China from 2001 to 2010. *Proc. Natl. Acad. Sci. USA* **2018**, *115*, 4039–4044. [[CrossRef](#)]
9. Zhang, Y.; Zhang, C.; Wang, Z.; Chen, Y.; Gang, C.; An, R.; Li, J. Vegetation Dynamics and Its Driving Forces from Climate Change and Human Activities in the Three-River Source Region, China from 1982 to 2012. *Sci. Total Environ.* **2016**, *563–564*, 210–220. [[CrossRef](#)]
10. Luo, Z.; Liu, E.; Qi, S.; Zhao, N.; Sun, Y. Flow Regime Changes in Three Catchments with Different Landforms Following Ecological Restoration in the Chinese Loess Plateau. *J. Arid Land* **2020**, *12*, 44–57. [[CrossRef](#)]
11. Zhao, A.; Zhang, A.; Lu, C.; Wang, D.; Wang, H.; Liu, H. Spatiotemporal Variation of Vegetation Coverage before and after Implementation of Grain for Green Program in Loess Plateau, China. *Ecol. Eng.* **2017**, *104*, 13–22. [[CrossRef](#)]
12. Muraoka, H.; Koizumi, H. Satellite Ecology (SATECO)—Linking Ecology, Remote Sensing and Micrometeorology, from Plot to Regional Scale, for the Study of Ecosystem Structure and Function. *J. Plant Res.* **2009**, *122*, 3–20. [[CrossRef](#)] [[PubMed](#)]

13. Fu, X.; Tang, C.; Zhang, X.; Fu, J.; Jiang, D. An Improved Indicator of Simulated Grassland Production Based on MODIS NDVI and GPP Data: A Case Study in the Sichuan Province, China. *Ecol. Indic.* **2014**, *40*, 102–108. [[CrossRef](#)]
14. Wilson, N.R.; Norman, L.M. Analysis of Vegetation Recovery Surrounding a Restored Wetland Using the Normalized Difference Infrared Index (NDII) and Normalized Difference Vegetation Index (NDVI). *Int. J. Remote Sens.* **2018**, *39*, 3243–3274. [[CrossRef](#)]
15. Li, P.; Wang, J.; Liu, M.; Xue, Z.; Bagherzadeh, A.; Liu, M. Spatio-Temporal Variation Characteristics of NDVI and Its Response to Climate on the Loess Plateau from 1985 to 2015. *CATENA* **2021**, *203*, 105331. [[CrossRef](#)]
16. Long, X.; Guan, H.; Sinclair, R.; Batelaan, O.; Facelli, J.M.; Andrew, R.L.; Bestland, E. Response of Vegetation Cover to Climate Variability in Protected and Grazed Arid Rangelands of South Australia. *J. Arid Environ.* **2019**, *161*, 64–71. [[CrossRef](#)]
17. Jiao, K.; Gao, J.; Wu, S. Climatic Determinants Impacting the Distribution of Greenness in China: Regional Differentiation and Spatial Variability. *Int. J. Biometeorol.* **2019**, *63*, 523–533. [[CrossRef](#)]
18. Zeng, F.-W.; Collatz, G.; Pinzon, J.; Ivanoff, A. Evaluating and Quantifying the Climate-Driven Interannual Variability in Global Inventory Modeling and Mapping Studies (GIMMS) Normalized Difference Vegetation Index (NDVI3g) at Global Scales. *Remote Sens.* **2013**, *5*, 3918–3950. [[CrossRef](#)]
19. Piao, S.; Wang, X.; Park, T.; Chen, C.; Lian, X.; He, Y.; Bjerke, J.W.; Chen, A.; Ciais, P.; Tømmervik, H.; et al. Characteristics, Drivers and Feedbacks of Global Greening. *Nat. Rev. Earth Environ.* **2020**, *1*, 14–27. [[CrossRef](#)]
20. Piao, S.; Wang, X.; Ciais, P.; Zhu, B.; Wang, T.; Liu, J. Changes in vegetation growth over Eurasia. *Glob. Chang. Biol.* **2011**, *17*, 3228–3239. [[CrossRef](#)]
21. Chen, B.; Xu, G.; Coops, N.C.; Ciais, P.; Innes, J.L.; Wang, G.; Myneni, R.B.; Wang, T.; Krzyzanowski, J.; Li, Q.; et al. Changes in Vegetation Photosynthetic Activity Trends across the Asia–Pacific Region over the Last Three Decades. *Remote Sens. Environ.* **2014**, *144*, 28–41. [[CrossRef](#)]
22. Ali, S.; HENCHIRI, M.; Yao, F.; Zhang, J. Analysis of Vegetation Dynamics, Drought in Relation with Climate over South Asia from 1990 to 2011. *Environ. Sci. Pollut. Res.* **2019**, *26*, 11470–11481. [[CrossRef](#)] [[PubMed](#)]
23. Dong, Y.; Yin, D.; Li, X.; Huang, J.; Su, W.; Li, X.; Wang, H. Spatial–Temporal Evolution of Vegetation NDVI in Association with Climatic, Environmental and Anthropogenic Factors in the Loess Plateau, China during 2000–2015: Quantitative Analysis Based on Geographical Detector Model. *Remote Sens.* **2021**, *13*, 4380. [[CrossRef](#)]
24. Zhao, A.; Zhang, A.; Liu, X.; Cao, S. Spatiotemporal Changes of Normalized Difference Vegetation Index (NDVI) and Response to Climate Extremes and Ecological Restoration in the Loess Plateau, China. *Appl. Clim.* **2018**, *132*, 555–567. [[CrossRef](#)]
25. Feng, X.; Fu, B.; Piao, S.; Wang, S.; Ciais, P.; Zeng, Z.; Lü, Y.; Zeng, Y.; Li, Y.; Jiang, X.; et al. Revegetation in China’s Loess Plateau Is Approaching Sustainable Water Resource Limits. *Nat. Clim. Chang.* **2016**, *6*, 1019–1022. [[CrossRef](#)]
26. Li, J.; Peng, S.; Li, Z. Detecting and Attributing Vegetation Changes on China’s Loess Plateau. *Agric. For. Meteorol.* **2017**, *247*, 260–270. [[CrossRef](#)]
27. Liu, Z.; Menzel, L. Identifying Long-Term Variations in Vegetation and Climatic Variables and Their Scale-Dependent Relationships: A Case Study in Southwest Germany. *Glob. Planet. Chang.* **2016**, *147*, 54–66. [[CrossRef](#)]
28. Tong, S.; Zhang, J.; Bao, Y.; Lai, Q.; Lian, X.; Li, N.; Bao, Y. Analyzing Vegetation Dynamic Trend on the Mongolian Plateau Based on the Hurst Exponent and Influencing Factors from 1982–2013. *J. Geogr. Sci.* **2018**, *28*, 595–610. [[CrossRef](#)]
29. Feng, X.; Fu, B.; Lu, N.; Zeng, Y.; Wu, B. How Ecological Restoration Alters Ecosystem Services: An Analysis of Carbon Sequestration in China’s Loess Plateau. *Sci. Rep.* **2013**, *3*, 2846. [[CrossRef](#)] [[PubMed](#)]
30. Ren, M.-E.; Shi, Y.-L. Sediment Discharge of the Yellow River (China) and Its Effect on the Sedimentation of the Bohai and the Yellow Sea. *Cont. Shelf Res.* **1986**, *6*, 785–810. [[CrossRef](#)]
31. Wang, J.; Dong, J.; Liu, J.; Huang, M.; Li, G.; Running, S.; Smith, W.; Harris, W.; Saigusa, N.; Kondo, H.; et al. Comparison of Gross Primary Productivity Derived from GIMMS NDVI3g, GIMMS, and MODIS in Southeast Asia. *Remote Sens.* **2014**, *6*, 2108–2133. [[CrossRef](#)]
32. Ali, Kuriqi; Abubaker; Kisi Long-Term Trends and Seasonality Detection of the Observed Flow in Yangtze River Using Mann-Kendall and Sen’s Innovative Trend Method. *Water* **2019**, *11*, 1855. [[CrossRef](#)]
33. Yang, X.; Xu, X.; Stovall, A.; Chen, M.; Lee, J. Recovery: Fast and Slow—Vegetation Response During the 2012–2016 California Drought. *J. Geophys. Res. Biogeosci.* **2021**, *126*, e2020JG005976. [[CrossRef](#)]
34. Fang, X.; Zhu, Q.; Ren, L.; Chen, H.; Wang, K.; Peng, C. Large-Scale Detection of Vegetation Dynamics and Their Potential Drivers Using MODIS Images and BFAST: A Case Study in Quebec, Canada. *Remote Sens. Environ.* **2018**, *206*, 391–402. [[CrossRef](#)]
35. Schultz, M.; Shapiro, A.; Clevers, J.; Beech, C.; Herold, M. Forest Cover and Vegetation Degradation Detection in the Kavango Zambezi Transfrontier Conservation Area Using BFAST Monitor. *Remote Sens.* **2018**, *10*, 1850. [[CrossRef](#)]
36. Ma, J.; Zhang, C.; Guo, H.; Chen, W.; Yun, W.; Gao, L.; Wang, H. Analyzing Ecological Vulnerability and Vegetation Phenology Response Using NDVI Time Series Data and the BFAST Algorithm. *Remote Sens.* **2020**, *12*, 3371. [[CrossRef](#)]
37. Geng, L.; Che, T.; Wang, X.; Wang, H. Detecting Spatiotemporal Changes in Vegetation with the BFAST Model in the Qilian Mountain Region during 2000–2017. *Remote Sens.* **2019**, *11*, 103. [[CrossRef](#)]
38. Li, K.; Zhang, B. Spatial and Temporal Evolution of Ecosystem Service Value in Shaanxi Province against the Backdrop of Grain for Green. *Forests* **2022**, *13*, 1146. [[CrossRef](#)]
39. Fu, B.; Liu, Y.; Lü, Y.; He, C.; Zeng, Y.; Wu, B. Assessing the Soil Erosion Control Service of Ecosystems Change in the Loess Plateau of China. *Ecol. Complex.* **2011**, *8*, 284–293. [[CrossRef](#)]

40. Norman, L.; Villarreal, M.; Pulliam, H.R.; Minckley, R.; Gass, L.; Tolle, C.; Coe, M. Remote Sensing Analysis of Riparian Vegetation Response to Desert Marsh Restoration in the Mexican Highlands. *Ecol. Eng.* **2014**, *70*, 241–254. [[CrossRef](#)]
41. Fraser, R.H.; Lantz, T.C.; Olthof, I.; Kokelj, S.V.; Sims, R.A. Warming-Induced Shrub Expansion and Lichen Decline in the Western Canadian Arctic. *Ecosystems* **2014**, *17*, 1151–1168. [[CrossRef](#)]
42. Yuan, M.; Wang, L.; Lin, A.; Liu, Z.; Li, Q.; Qu, S. Vegetation Green up under the Influence of Daily Minimum Temperature and Urbanization in the Yellow River Basin, China. *Ecol. Indic.* **2020**, *108*, 105760. [[CrossRef](#)]
43. Tian, H.; Cao, C.; Chen, W.; Bao, S.; Yang, B.; Myneni, R.B. Response of Vegetation Activity Dynamic to Climatic Change and Ecological Restoration Programs in Inner Mongolia from 2000 to 2012. *Ecol. Eng.* **2015**, *82*, 276–289. [[CrossRef](#)]
44. Mueller, T.; Dressler, G.; Tucker, C.; Pinzon, J.; Leimgruber, P.; Dubayah, R.; Hurtt, G.; Böhning-Gaese, K.; Fagan, W. Human Land-Use Practices Lead to Global Long-Term Increases in Photosynthetic Capacity. *Remote Sens.* **2014**, *6*, 5717–5731. [[CrossRef](#)]
45. Wen, Z.; Wu, S.; Chen, J.; Lü, M. NDVI Indicated Long-Term Interannual Changes in Vegetation Activities and Their Responses to Climatic and Anthropogenic Factors in the Three Gorges Reservoir Region, China. *Sci. Total Environ.* **2017**, *574*, 947–959. [[CrossRef](#)]
46. Shi, S.; Yu, J.; Wang, F.; Wang, P.; Zhang, Y.; Jin, K. Quantitative Contributions of Climate Change and Human Activities to Vegetation Changes over Multiple Time Scales on the Loess Plateau. *Sci. Total Environ.* **2021**, *755*, 142419. [[CrossRef](#)]
47. Tesfaye, S.; Taye, G.; Birhane, E.; van der Zee, S.E.A.T.M. Spatiotemporal Variability of Ecosystem Water Use Efficiency in Northern Ethiopia during 1982–2014. *J. Hydrol.* **2021**, *603*, 126863. [[CrossRef](#)]
48. Zhang, S.; Yang, D.; Yang, Y.; Piao, S.; Yang, H.; Lei, H.; Fu, B. Excessive Afforestation and Soil Drying on China’s Loess Plateau. *J. Geophys. Res. Biogeosci.* **2018**, *123*, 923–935. [[CrossRef](#)]
49. Li, S.; Liang, W.; Fu, B.; Lü, Y.; Fu, S.; Wang, S.; Su, H. Vegetation Changes in Recent Large-Scale Ecological Restoration Projects and Subsequent Impact on Water Resources in China’s Loess Plateau. *Sci. Total Environ.* **2016**, *569–570*, 1032–1039. [[CrossRef](#)]